Unsteady numerical estimation of the aerodynamic loads of the Krueger flap

Marius Gabriel COJOCARU*,[1], Mihai Leonida NICULESCU[1], Claudiu VADEAN[1]

*Corresponding author
*,[1]INCAS – National Institute for Aerospace Research "Elie Carafoli"
B-dul Iuliu Maniu 220, Bucharest 061126, Romania
mcojocaru@incas.ro

DOI: 10.13111/2066-8201.2012.4.1.1

Abstract: *The aim of this paper is to study the unsteady aerodynamic interaction between a Krueger flap and a three-element airfoil using the finite volume method to solve the Unsteady Reynolds-Averaged Navier-Stokes equations. For a better understanding of this unsteady interaction, the Krueger flap is placed at different positions. Our results clearly show that the airfoil's aerodynamic performance and the pressure distributions are strongly influenced by the Krueger flap position.*

Key Words: *Krueger flap, unsteady aerodynamic loads, CFD, parallel computing*

1. INTRODUCTION

The Krueger flaps, invented by W. Krüger in 1943 are lift enhancement devices that may be fitted to the leading edge of an airplane wing. Unlike slats or drooped leading edges, the main wing upper surface and its nose is not changed. Instead, a portion of the lower wing is rotated out in front of the main wing leading edge. Krueger flaps, hinged at their leading edges, hinge forwards from the under surface of the wing, increasing the wing camber and maximum coefficient of lift at take-off and landing. However, the unsteady interaction between Krueger flap and airfoil generates the unsteady aerodynamic loads and fatigue, which decreases their life. For this reason, we have considered that it is useful to study this interaction. Furthermore, there is very little available information about this topic.

2. GOVERNING EQUATIONS

For a two-dimensional stationary Cartesian coordinate system, the unsteady Reynolds-averaged Navier-Stokes equations using the Favre averaging (a mass-weighted averaging) could be written in the conservative form as [1-3]

$$\frac{\partial Q}{\partial t}+\frac{\partial\left(F_x-G_x\right)}{\partial x}+\frac{\partial\left(F_y-G_y\right)}{\partial y}=S \tag{1}$$

where

$$Q=\begin{bmatrix}\rho\\ \rho u\\ \rho v\\ \rho E\end{bmatrix}\quad F_x=\begin{bmatrix}\rho u\\ \rho u^2+p\\ \rho uv\\ \rho uH\end{bmatrix}\quad F_y=\begin{bmatrix}\rho v\\ \rho vu\\ \rho v^2+p\\ \rho vH\end{bmatrix} \tag{2}$$

If one assumes that the fluid is Newtonian and the thermal boundary layer is neglected, the diffusive flux G may be written as

$$G_x = \begin{bmatrix} 0 \\ \tau_{xx}^{tot} \\ \tau_{xy}^{tot} \\ u\tau_{xx}^{tot} + v\tau_{xy}^{tot} + \alpha\dfrac{\partial T}{\partial x} \end{bmatrix} \quad G_y = \begin{bmatrix} 0 \\ \tau_{xy}^{tot} \\ \tau_{yy}^{tot} \\ u\tau_{xy}^{tot} + v\tau_{yy}^{tot} + \alpha\dfrac{\partial T}{\partial y} \end{bmatrix} \tag{3}$$

According to the Boussinesq hypothesis, the shear stresses τ^{tot} may be written as

$$\tau_{xx}^{tot} = \frac{2}{3}(\mu + \mu_t)\left(2\frac{\partial u}{\partial x} - \frac{\partial v}{\partial y}\right) \quad \tau_{yy}^{tot} = \frac{2}{3}(\mu + \mu_t)\left(2\frac{\partial v}{\partial y} - \frac{\partial u}{\partial x}\right)$$
$$\tau_{xy}^{tot} = \frac{2}{3}(\mu + \mu_t)\left(\frac{\partial u}{\partial y} + \frac{\partial v}{\partial x}\right) \tag{4}$$

The Sutherland's formula could be used to determine the dynamic viscosity μ as a function of temperature, while the eddy viscosity μ_t is computed with a turbulence model.

For gases, the external force f_e due to the gravitational acceleration is very small, therefore it can be neglected.

Moreover, we can assume that the thermal conductivity is the single heat source, therefore the source term S becomes null

$$S = 0 \tag{5}$$

The pressure is obtained from the equation of state of ideal gas

$$p = \rho RT \tag{6}$$

Furthermore, we could assume that air is a perfect gas; therefore

$$e = \frac{R}{\gamma - 1}T \quad h = \frac{\gamma R}{\gamma - 1}T \tag{7}$$

3. TURBULENCE MODEL

In 1995, T-H Shih et al. [4] have published the realizable k-ε turbulence model, which is an original modification to the standard k-ε turbulence model [5]. The realizable k-ε model differs from the standard k-ε model in two important ways. Firstly, it contains an alternative formulation for the turbulent viscosity. Secondly, a modified transport equation for the dissipation rate ε has been derived from an exact equation for the transport of the mean-square vorticity fluctuation.

The unsteady two-dimensional transport equations of the realizable k-ε turbulence model neglecting the buoyancy effects could be written in the conservative form as

$$\frac{\partial}{\partial t}(\rho k) + \frac{\partial}{\partial x}(\rho k u) + \frac{\partial}{\partial y}(\rho k v) =$$
$$\frac{\partial}{\partial x}\left[\left(\mu + \frac{\mu_t}{\sigma_k}\right)\frac{\partial k}{\partial x}\right] + \frac{\partial}{\partial y}\left[\left(\mu + \frac{\mu_t}{\sigma_k}\right)\frac{\partial k}{\partial y}\right] + G_k - Y_M \tag{8}$$

$$\frac{\partial}{\partial t}(\rho\varepsilon)+\frac{\partial}{\partial x}(\rho\varepsilon u)+\frac{\partial}{\partial y}(\rho\varepsilon v)=$$
$$\frac{\partial}{\partial x}\left[\left(\mu+\frac{\mu_t}{\sigma_\varepsilon}\right)\frac{\partial\varepsilon}{\partial x}\right]+\frac{\partial}{\partial y}\left[\left(\mu+\frac{\mu_t}{\sigma_\varepsilon}\right)\frac{\partial\varepsilon}{\partial y}\right]+\rho C_1 S\varepsilon-\rho C_2\frac{\varepsilon^2}{k+\sqrt{\frac{\mu}{\rho}}\varepsilon} \tag{9}$$

where

$$C_1=\max\left[0.43,\frac{\eta}{\eta+5}\right]\quad \eta=S\frac{k}{\varepsilon}\quad S=\sqrt{2\left[\left(\frac{\partial u}{\partial x}\right)^2+\left(\frac{\partial v}{\partial y}\right)^2\right]+\left(\frac{\partial u}{\partial y}+\frac{\partial v}{\partial x}\right)^2} \tag{10}$$

In the above equations, G_k represents the generation of turbulence kinematic energy due to mean velocity gradients, calculated as in the standard k-ε turbulence model while Y_M is the contribution of the fluctuating dilatation in compressible turbulence to the overall dissipation rate

$$Y_M=2\rho\varepsilon M_t^2 \tag{11}$$

where M_t is the turbulent Mach number, defined as

$$M_t=\sqrt{\frac{k}{a^2}}=\sqrt{\frac{k}{\gamma RT}} \tag{12}$$

As in the standard k-ε turbulence model, the eddy viscosity is computed from

$$\mu_t=\rho C_\mu\frac{k^2}{\varepsilon} \tag{13}$$

but C_μ is no longer constant. It is computed from

$$C_\mu=\frac{1}{A_0+A_S\frac{kU^*}{\varepsilon}} \tag{14}$$

where

$$A_0=4.04\quad A_S=\sqrt{6}\cos\phi\quad \phi=\frac{1}{3}\arccos\left(\sqrt{6}W\right)\quad U^*=\sqrt{\frac{S^2}{2}+\tilde{\Omega}_{ij}\tilde{\Omega}_{ij}} \tag{15}$$

For a two-dimensional stationary Cartesian coordinate system, the square of mean rate-of rotation tensor $\tilde{\Omega}_{ij}$ and W have the following expressions:

$$\tilde{\Omega}_{ij}\tilde{\Omega}_{ij}=\frac{1}{2}\left(\frac{\partial u}{\partial y}-\frac{\partial v}{\partial x}\right)^2\quad W=\frac{S_{ij}}{\frac{S}{\sqrt{2}}}=\frac{\frac{\partial u}{\partial x}+\frac{\partial v}{\partial y}+\frac{\partial u}{\partial y}+\frac{\partial v}{\partial x}}{\frac{S}{\sqrt{2}}} \tag{16}$$

The model constants C_2, σ_k and σ_ε have been established to ensure that the model performs well for certain canonical flows:

$$C_2=1.9\quad \sigma_k=1.0\quad \sigma_\varepsilon=1.2 \tag{17}$$

4. NUMERICAL SIMULATION

The numerical simulations of the two-dimensional viscous flow were carried on a multi-element airfoil shown in Fig. 1, with an in-house code developed by INCAS, which is based on finite volume method where each unknown takes an average value on each discretization cell. The mesh for which, the results are given, has about 26 000 cells. The height of the first row of cells near airfoil as shown in Fig.2 is chosen so that the averaged dimensionless distance y^+ is about 200.

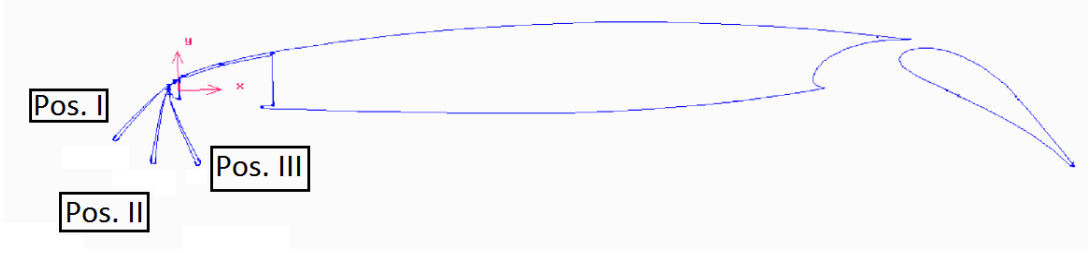

Fig. 1 – Configuration for the Krueger flap positions and rotation center

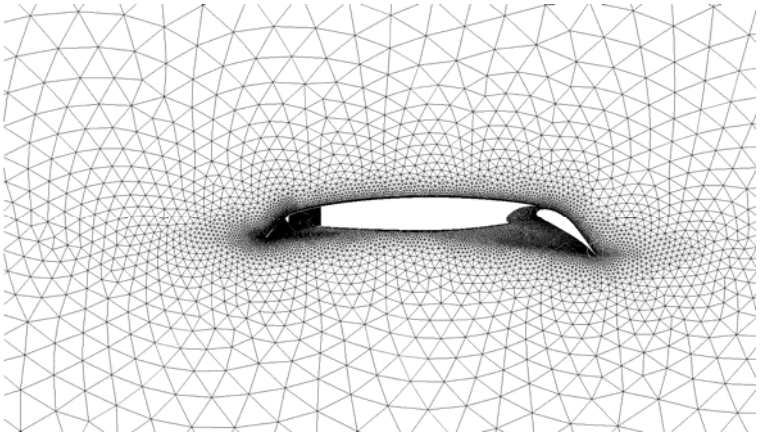

Fig. 2 – Detail of the mesh, near airfoil

Because the realizable k-ε model is a high-Reynolds turbulence model, we used the non-equilibrium wall functions [6] that are suitable in complex flows with separations and reattachments.

In order to decrease the computational time, impressively, the discretization is made with an implicit formulation. To take into account the physical properties of flow, the convective fluxes are discretized with the Roe scheme, which is a Godunov-type scheme [7-10]. The simulation is carried out with a compressible Navier-Stokes (density based) solver, with an implicit formulation and a dual-time marching algorithm and a fixed time step of dt = 1e-4 s, for accuracy reasons.

5. CASE SETUP

The numerical simulations have been performed within the following free-stream conditions: Pressure = 101325 Pa. Temperature = 300 K. Turbulence intensity = 0.5 %. Viscosity ratio = 0.2. Angle of Attack (AoA) = from -10º to +20º.
The velocity is computed from a condition of Mach = 0.2 and corresponds to V =70 m/s.

The reference values for the computation of the forces and moment coefficients are: Aria = 0.23 m^2. Length = 0.23m. Density = 1.177kg/m^3. Temperature = 300 K. Velocity = 70 m/s. Specific heats ratio = 1.4. Viscosity = 1.789e-5 kg/m·s.

6. RESULTS

The results for the unsteady simulations are given in the tables below for the minimum and maximum of the coefficients, and also for their frequencies. Also, it should be noted that whenever a result is omitted in the table or a NA is recorded it is a case of either a constant value of the coefficient or a numerical oscillation is recorded in the numerical solver, respectively.

To clarify we present the case of the oscillations of the lift force coefficient at α = -6º and α = -10º, from where we can deduce three different possibilities. First, if the lift coefficient is almost constant then in the tables 1-3 that value is recorded and in the frequency column a NA is recorded, or if the lift coefficient is oscillating as a result of a numerical error and is not correlated to a physical phenomenon, than again only a mean value of the lift coefficient is recorded and a NA for the frequency. Second, if there is just one amplitude for the variation of the lift coefficient (case of α = -10º) then that amplitude and its corresponding frequency are recorded in the table. Last, if the amplitudes of the oscillations are roughly of the same order of magnitude (case of α = -6º), then we will write in the table the values and frequency for the highest amplitude.

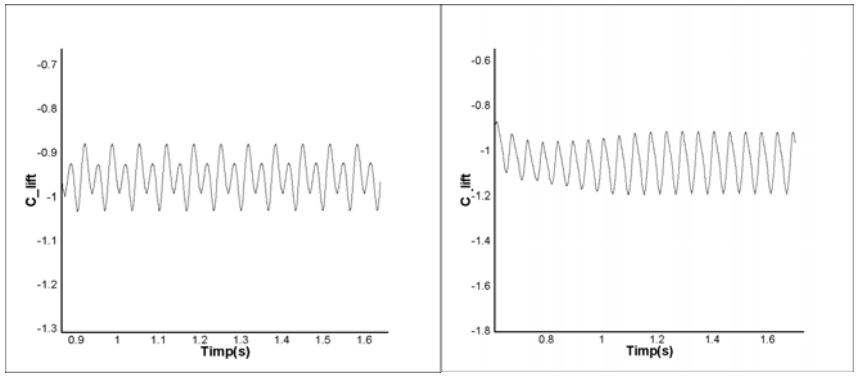

Fig. 3 - Time variation of the lift force coefficient at α = -6º(left) and α = -10º(right).

A physical explanation of these kinds of behaviors is given by analyzing the instantaneous flow field at several cases of interest, α = -6º, α = 0º and α = +6º.

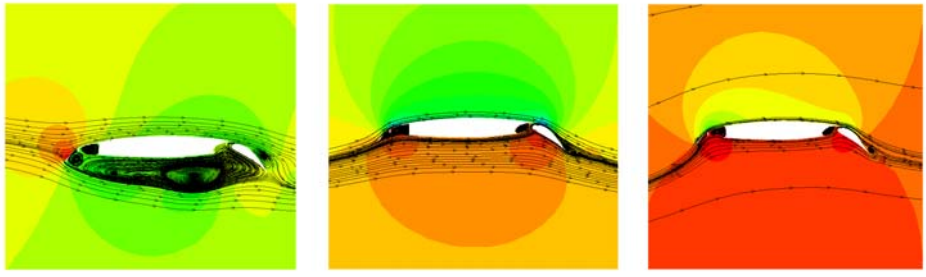

Fig. 4 - Pressure coefficient contours and streamlines at α = -6º(left), α = 0º(middle) and α = +6º(right)

It can be seen in this case (α = -6º) that the recirculation zone extends on the whole lower-surface and the vortex shedding mechanism behind the Krueger flap is a periodic one and can be described by the superposition of several frequencies, corresponding to vortices of roughly the same size.

In the case of α = 0º the recirculation area on the lower-surface has disappeared and the vortices behind the Krueger flap are smaller and also their corresponding frequency is increased (while the amplitude of the coefficients has decreased) compared to the previous case (α = -6º).

Concerning the case of α = +6º, the flow is almost perfectly attached to the Krueger flap and we expect to see higher frequencies and smaller amplitudes than in any of the previous cases. Also the amplitudes of the coefficients oscillations have a quasi-constant appearance.

- **Position I**

Table 1 - Coefficients for Position I

AoA	Cz_min	Cz_max	Cx_min	Cx_max	Cm_min	Cm_max	Freq. (Hz)
-10	-1.2095	-0.936	0.858	1.107	0.616	0.773	16
-8	-1.193	-0.920	0.844	1.095	0.618	0.777	17
-6	-1.032	-0.881	0.809	0.947	0.609	0.699	30
-4	-0.814	-0.791	0.732	0.752	0.573	0.588	33
-2	0.194	0.225	-0.202	-0.171	-0.015	0.0027	140
0	0.752	0.765	-0.7385	-0.725	-0.404	-0.397	90
2	1.205	1.215	-1.240	-1.229	-0.768	-0.761	140
4	1.651	1.656	-1.8408	-1.8359	-1.2083	-1.2055	100
6	2.138	2.139	-2.5246	-2.523	-1.7044	-1.7034	80
8	---	2.6371	---	-3.1408	---	-2.1367	NA
10	---	2.8155	---	-3.5765	---	-2.3567	NA
12	2.986	2.994	-3.7039	-3.699	-2.4348	-2.4315	34
14	2.940	2.956	-3.726	-3.707	-2.441	-2.4297	27
16	2.701	2.880	-3.6143	-3.4185	-2.361	-2.24	20
18	2.697	3.066	-3.8295	-3.3615	-2.4411	-2.1574	16
20	1.878	2.596	-3.281	-2.335	-2.0631	-1.484	13

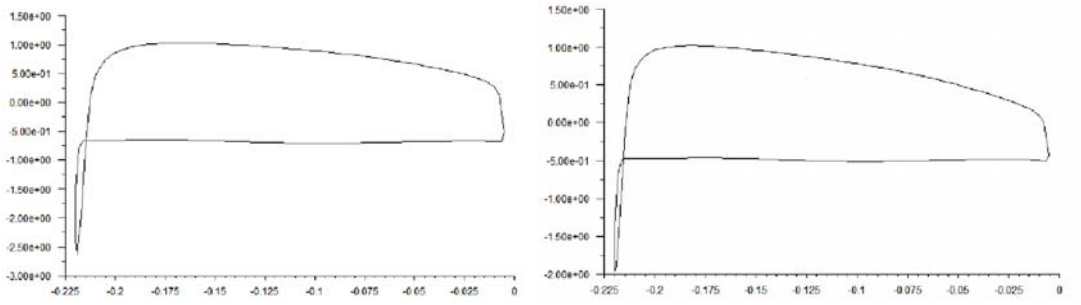

Fig. 5 - C_p distribution on the Krueger flap at α = -6º (left) and at α = -4º (right).

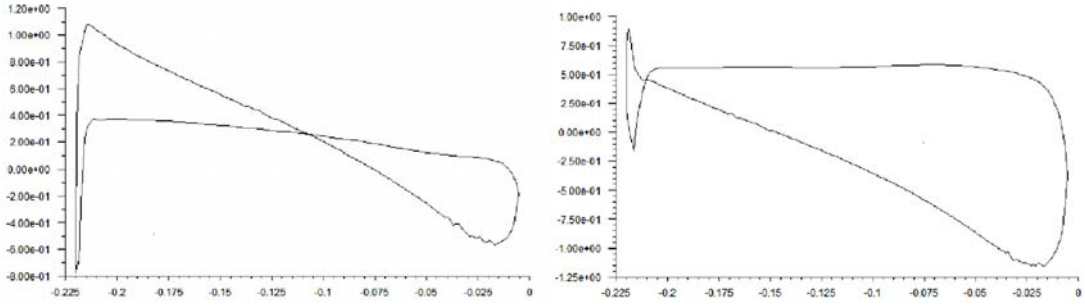

Fig. 6 - C_p distribution on the Krueger flap at α = -2º (left) and at α = 0º (right).

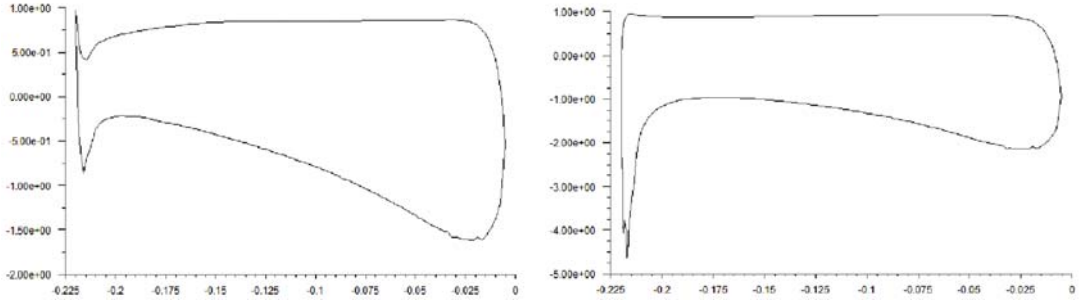

Fig. 7 - C_p distribution on the Krueger flap at α = 2º (left) and at α = 4º (right).

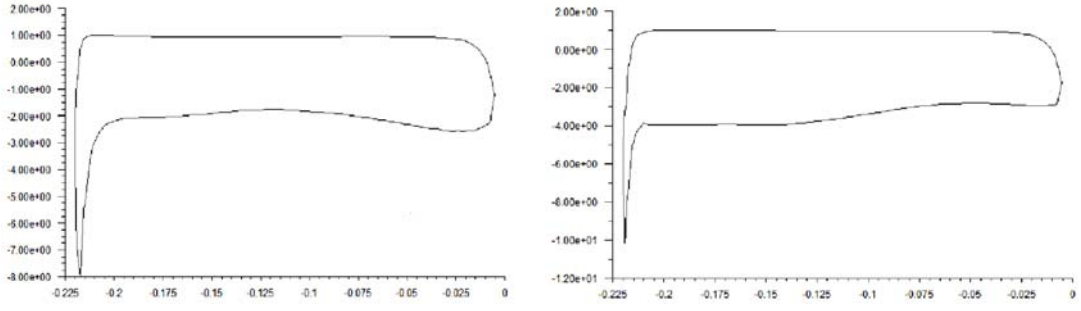

Fig. 8 - C_p distribution on the Krueger flap at α = 6º (left) and at α = 8º (right).

- **Position II**

Similarly to the Position I case a correlation on the vortex shedding behind the Krueger flap and the time variation of the coefficients can be summarized in the table below.

Table 2 - Coefficients for Position II

AoA	Cz_min	Cz_max	Cx_min	Cx_max	Cm_min	Cm_max	Freq. (Hz)
-10	-0.379	-0.287	1.1146	1.4554	0.5148	0.6545	9
-8	-0.390	-0.311	1.1912	1.5043	0.5511	0.6823	20
-6	-0.382	-0.314	1.1764	1.4859	0.5566	0.6892	16
-4	-0.339	-0.318	1.2565	1.3358	0.6018	0.6359	30
-2	-0.294	-0.265	1.0656	1.1753	0.5370	0.5853	32
0	-0.130	-0.129	0.5265	0.5289	0.3437	0.3448	61
2	---	0.018	---	0.0141	---	0.1426	NA
4	0.113	0.115	-0.3565	-0.3506	-0.0252	-0.0218	76
6	0.230	0.232	-0.8111	-0.8034	-0.2341	-0.2288	73
8	0.367	0.368	-1.3643	-1.3594	-0.4862	-0.4837	69
10	0.488	0.489	-1.9432	-1.9365	-0.7706	-0.7671	67
12	0.565	0.565	-2.5523	-2.5482	-1.0981	-1.096	64
14	0.611	0.611	-3.2202	-3.2173	-1.4579	-1.4566	62
16	---	---	---	---	---	---	NA
18	---	---	---	---	---	---	NA
20	0.684	0.688	-3.9807	-3.9521	-1.9386	-1.9216	22

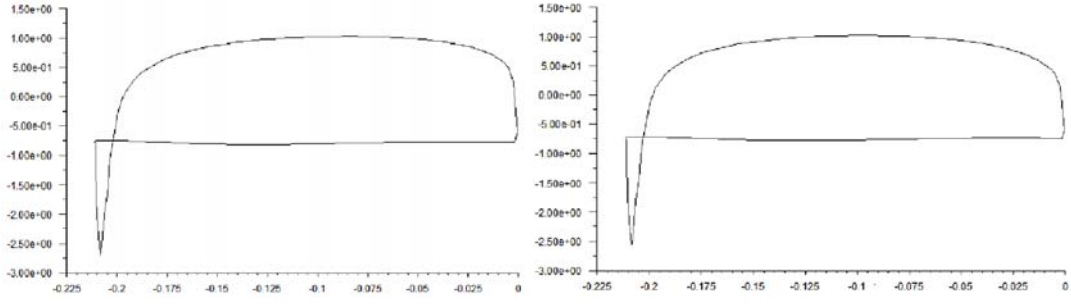

Fig. 9 - C_p distribution on the Krueger flap at α = -6º (left) and at α = -4º (right).

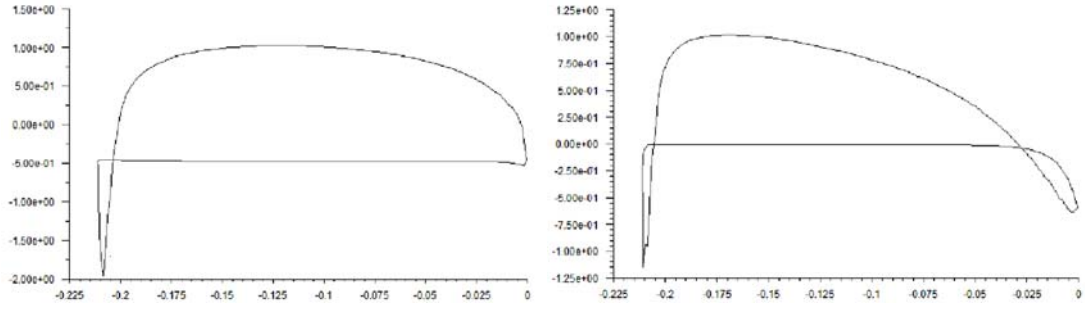

Fig. 10 - C_p distribution on the Krueger flap at α = -2º (left) and at α = 0º (right).

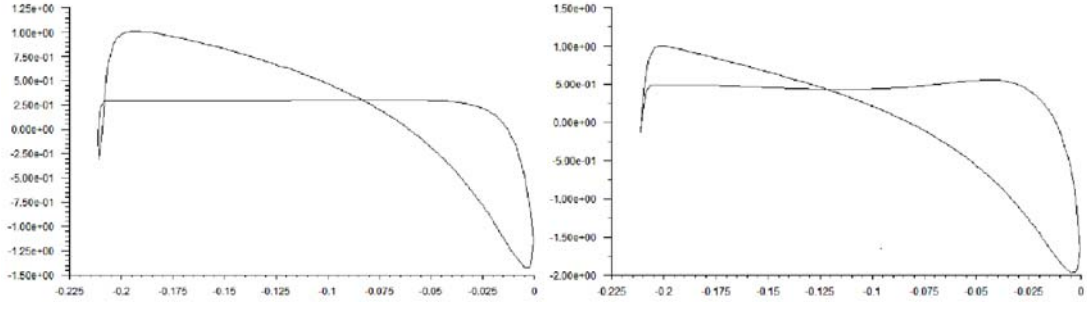

Fig. 11- C_p distribution on the Krueger flap at α = 2º (left) and at α = 4º (right).

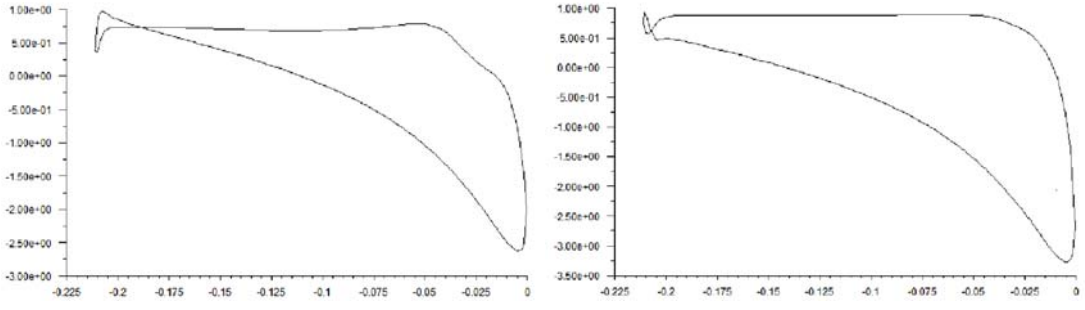

Fig. 12 - C_p distribution on the Krueger flap at α = 6º (left) and at α = 8º (right).

- **Position III**

Similarly to the Position I and Position II case a correlation on the vortex shedding behind the Krueger flap and the time variation of the coefficients can be summarized in the table below.

Table 3 - Coefficients for Position III

AoA	Cz_min	Cz_max	Cx_min	Cx_max	Cm_min	Cm_max	Freq.(Hz)
-10	0.2484	0.3072	0.8700	1.0695	0.3231	0.4003	18
-8	0.2636	0.3278	0.9174	1.1351	0.3473	0.4312	19
-6	0.2643	0.3034	0.9404	1.0747	0.3514	0.4305	20

-4	0.2896	0.3212	0.9974	1.0954	0.4034	0.4356	27
-2	0.2765	0.2978	0.9494	1.0213	0.3866	0.4151	33
0	0.2172	0.2242	0.7906	0.8149	0.3320	0.3419	45
2	---	0.1195	---	0.3922	---	0.2332	NA
4	---	0.0346	---	0.0782	---	0.1294	NA
6	---	-0.0447	---	-0.2058	---	0.0420	NA
8	---	-0.1005	---	-0.4212	---	-0.0380	NA
10	---	-0.2110	---	-0.7902	---	-0.2029	NA
12	---	-0.3254	---	-1.1568	---	-0.3612	NA
14	-0.3551	-0.3088	-1.2475	-1.1060	-0.4045	-0.3424	4
16	-0.4065	0.0161	-1.3972	0.0121	-0.4782	0.0996	2
18	-0.1673	-0.1035	-0.6291	-0.4126	-0.1548	-0.0681	15
20	-0.2406	-0.1638	-0.8647	-0.6121	-0.2647	-0.571	13

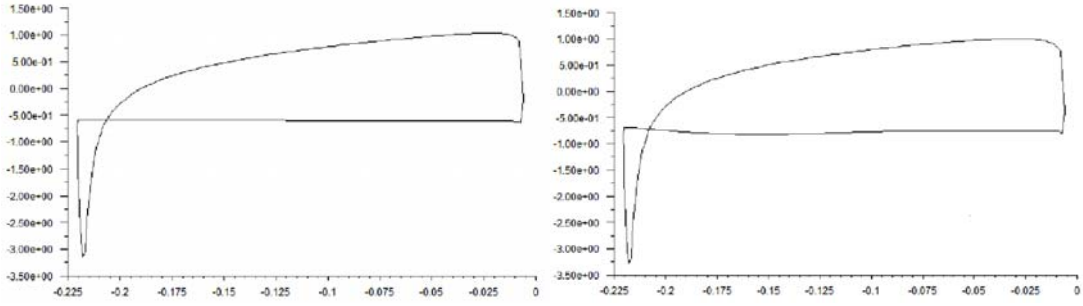

Fig. 13 - C_p distribution on the Krueger flap at α = -6º (left) and at α = -4º (right).

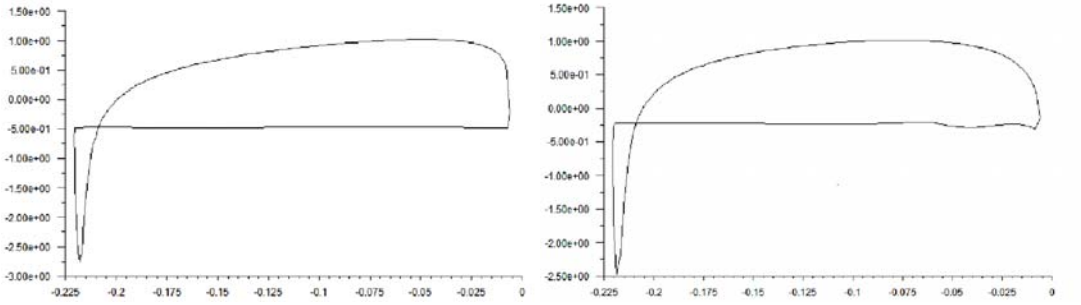

Fig. 14 - C_p distribution on the Krueger flap at α = -2º (left) and at α = 0º (right).

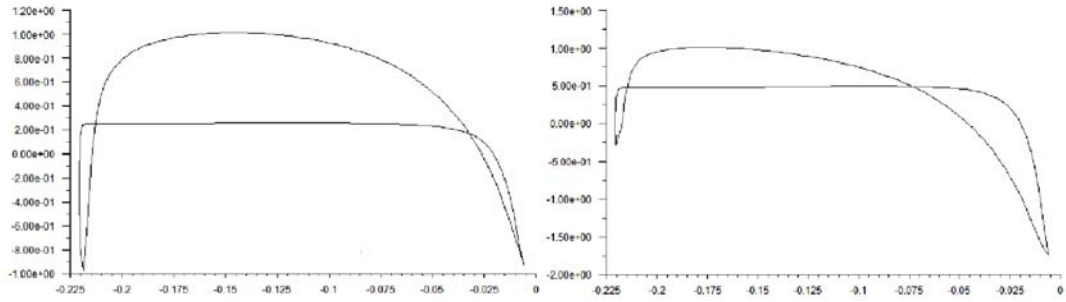

Fig. 15- C_p distribution on the Krueger flap at $\alpha = 2^o$ (left) and at $\alpha = 4^o$ (right).

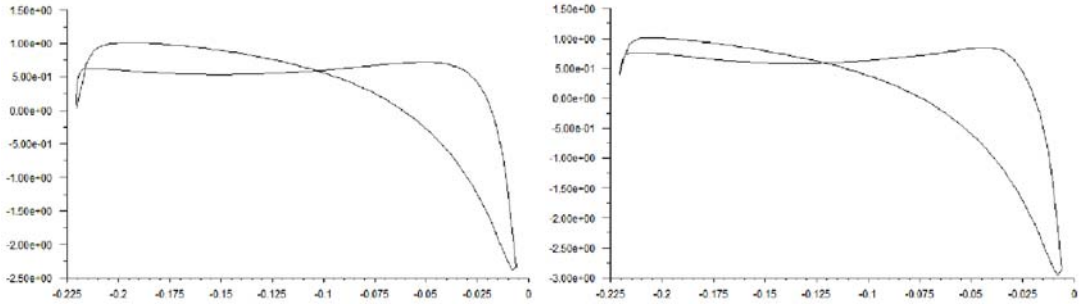

Fig. 16 - C_p distribution on the Krueger flap at $\alpha = 6^o$ (left) and at $\alpha = 8^o$ (right).

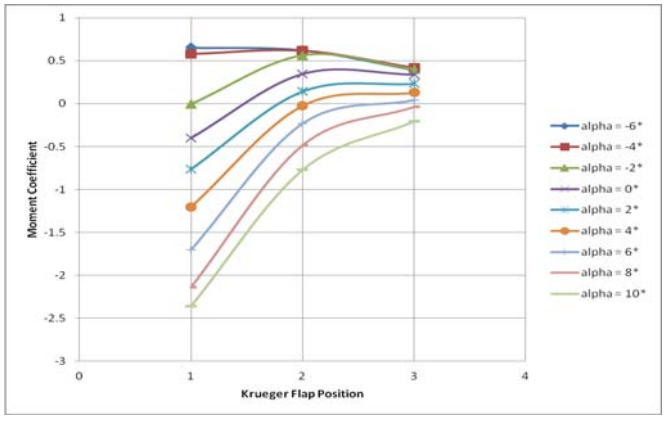

Fig. 17 - Cm variation with the position of the Krueger flap for α in [-6,10] deg

6. CONCLUSIONS

The design of the actuator system for the Krueger flap must take into account the unsteady loads induced in the structure, especially since the numerical results clearly show that the flow is strongly unsteady past the Krueger flap even at moderate angles of attack as shown in Fig. 3 and Tables 1-3. This unsteady flow could trigger the appearance of fatigue and even noise, generated by flow induced oscillations. However, the Krueger flap is a main element of wing configurations of many modern aircraft because it increases the lift impressively during take-off and landing. 3D computations are necessary to completely analyse this configuration as it would be very useful to try to mitigate the effects of the unsteady aerodynamic loads caused by the Krueger flap.

REFERENCES

[1] D. C. Wilcox, *Turbulence Modeling for CFD*, DCW Industries, Inc., La Canada, California, 1998.
[2] S. Dănăilă and C. Berbente, *Metode Numerice în Dinamica Fluidelor*, Editura Academiei Române, 2003.
[3] C. Hirsch, *Numerical Computation of Internal and External Flow, Volume 2: Computational Methods for Inviscid and Viscous Flows*, John Wiley and Sons, New York, 1990.
[4] T.-H. Shih, W. W. Liou, A. Shabbir, Z. Yang, and J. Zhu, A new k-ε eddy-viscosity model for high Reynolds number turbulent flows – Model development and validation, *Computers and Fluids*, vol. **24**, issue 3, pp. 227-238, ISSN: 0045-7930, 1995.
[5] B. E. Launder and D. B. Spalding, *Lectures in mathematical models of turbulence*, Academic Press, London, England, 1972.
[6] S.-E. Kim and D. Choudhury, *A near-wall treatment using wall functions sensitized to pressure gradient*, in ASME FED Vol. **217**, Separated and Complex Flows, ASME, 1995.
[7] B. v. Leer, Towards the ultimate conservative difference scheme. V. A second-order sequel to Godunov's method, *Journal of Computational Physics*, Vol. **32**, Issue 1, pp. 101-136, ISSN: 0021-9991, 1979.
[8] P. L. Roe, The use of Riemann problem in finite difference schemes, *Lecture Notes in Physics*, Vol. **141**, pp. 354-359, 1980.
[9] P. L. Roe, Approximate Riemann solvers, parameter vectors, and difference schemes, *Journal of Computational Physics*, Vol. **43**, Issue 2, pp. 357-372, ISSN: 0021-9991, 1981.
[10] P. L. Roe, Characteristic-based schemes for the Euler equations, *Annual Review of Fluid Mechanics*, Vol. **18**, pp. 337-365, 1986.